Stochastic forcing for sub-grid scale models in wall-modeled large-eddy simulation

Simon Blanchard, Nicolas Odier, Laurent Gicquel, Bénédicte Cuenot, Franck Nicoud

Stochastic forcing for sub-grid scale models in wall-modeled large-eddy simulation

S. Blanchard,[1,2,a)] N. Odier,[2] L. Gicquel,[2] B. Cuenot,[2] and F. Nicoud[3]

AFFILIATIONS

[1]CNES, Launchers Directorate, 52 rue Jacques Hillairet, 75612 Paris Cedex, France
[2]CERFACS, 42 Avenue Gaspard Coriolis, Toulouse Cedex 1 31057, France
[3]IMAG, University of Montpellier, CNRS, 34090 Montpellier, France

[a)]Author to whom correspondence should be addressed: blanchard@cerfacs.fr

ABSTRACT

In the framework of wall-modeled large-eddy simulation (WMLES), the problem of combining sub-grid scale (SGS) models with the standard wall law is commonly acknowledged and expressed through multiple undesired near-wall behaviors. In this work, it is first observed that the static Smagorinsky model predicts efficiently the wall shear stress in a wall-modeled context, while more advanced static models like wall-adapting local eddy (WALE) viscosity or Sigma with proper cubic damping fail. It is, however, known that Smagorinsky is overall too dissipative in the bulk flow and in purely sheared flows, whereas the two other models are better suited for near-wall flows. The observed difficulty comes from the fact that the SGS model relies on the filtered velocity gradient tensor that necessarily comes with large errors in the near-wall region in the context of WMLES. Since the first off-wall node is usually located in the turbulent zone of the boundary layer, the turbulent structures within the first cell are neither resolved by the grid nor represented by the SGS model, which results in a lack of turbulent activity. In order to account for these subgrid turbulent structures, a stochastic forcing method derived from Reynolds-averaged Navier–Stokes (RANS) turbulence models is proposed and applied to the velocity gradients to better estimate the near-wall turbulent viscosity while providing the missing turbulent activity usually resulting from the WMLES approach. Based on such corrections, it is shown that the model significantly improves the wall shear stress prediction when used with the WALE and Sigma models.

I. INTRODUCTION

In fluid dynamics, turbulence is a complex phenomenon characterized by the motion, the creation, and the dissipation of different scales, from the largest to the smallest eddies. Today, direct numerical simulation (DNS) allows one to numerically study with the highest precision turbulence because the mesh is fine enough to capture the smallest eddies (Kolmogorov scale) without any need of modeling. However, this requires huge computational resources: DNS is therefore restricted to academic cases like homogeneous isotropic turbulence (HIT) or channel flows at moderate Reynolds numbers. When dealing with industrial applications, DNS is too expensive and modeling is needed. In this specific context, the large-eddy simulation (LES) modeling approach has shown successes by resolving the largest structures while modeling the smallest ones that are spatially filtered by the grid size and known to be computationally expensive to resolve.[1] The smallest eddies are therefore modeled by a so-called sub-grid scale (SGS) model to close the problem, which accounts for the energy transfer between the resolved and the modeled scales, following the well-known Kolmogorov energy cascade theory.[2]

Even if LES has proved its capability to compute complex turbulent flows,[3,4] wall-bounded flows remain a challenge and induce a large computational cost. Indeed, with increasing Reynolds numbers, small turbulent structures in the near-wall region still lead to strong mesh requirements, and the cost of LES approaches the cost of DNS. Chapman[5] estimated that the inner layer of the boundary layer (about 20% of its height) scales with $Re^{1.8}$. This order of magnitude has been updated by Choi and Moin,[6] where the authors suggest even a higher cost. In industrial flows where the Reynolds number can easily reach 1×10^6, this makes LES unaffordable to accurately resolve the boundary layer characteristic dynamics, that is, with the so-called wall-resolved LES (WRLES) approach.

To alleviate the cost induced by this specific flow region, the concept of wall-modeled LES (WMLES) is often put forward. Several ways currently exist to model wall flows, and the reader is refereed to

Larsson *et al.*[7] and Bose and Park[8] for recent overviews of the available methods. Among them, a widely used approach is the wall stress model, where LES is used everywhere in the domain with dedicated wall functions and models. Wall stress models can be developed in a physical sense, trying to reproduce the real fluid behavior known thanks for experiments or DNS, such as the classic log-law.[9] However, the context of WMLES is also prone to numerical errors, and mathematical-based models are developed to circumvent this problem, like in Nicoud *et al.*[10] This article focuses on wall stress models, which we refer to as WMLES from here on.

This latter framework however leads to specific difficulties related to the coupling between wall laws and SGS models. This point has been recently discussed in Rezaeiravesh *et al.*,[11] Bae *et al.*,[12] and Vanna.[13] In those works, the authors indicate that the SGS contribution must be non-zero for a coarse grid at the wall. This means that the choice of the SGS model is a crucial parameter for the wall stress prediction and has consequences on the so-called log-layer mismatch problem.[14–16] This well-known phenomenon leads to potentially large errors on the prediction of the wall shear stress and can indeed come from not only SGS influence, but also numerical scheme choice[17] or the treatment of the boundary condition.[18] In the present study, one focuses on SGS models making use of the gradient hypothesis and more specifically the static Smagorinsky,[19] wall-adapting local eddy viscosity (WALE),[20] and Sigma[21] models. The static Smagorinsky model has been derived for isotropic turbulence, while WALE and Sigma have been derived in a wall-resolved context, to provide an accurate turbulent viscosity behavior close to the wall. In a wall-modeled context, Jaegle *et al.*[22] however indicated that the standard wall law gives better results in combination with the Smagorinsky model because it provides more turbulent viscosity at the wall. On the contrary, WALE and Sigma both have the property to vanish for pure shear flows and follow the physical y^3 damping function near the wall.

However, although the Smagorinsky model has the desired property of providing a non-zero viscosity at the wall in WMLES, it is known to be too dissipative in the bulk flow, decreasing the overall LES quality in either WRLES or WMLES context. WALE and Sigma on the other hand show usually good results in the bulk flow, in both non-reactive and reactive cases whenever subject to pure shear, rotation, and contraction. In order to provide accurate LES results both in the bulk flow and in the near-wall region in a wall-modeled context, consistent SGS models, and wall-law coupling procedures must therefore be developed. This idea is not new, and the literature provides several examples investigating this problem.[13,23–26] Note also that the coupling of SGS models with other kind of physics is a general concern in LES, for example, in the case of particle-laden flows (including the near-wall problematic), as suggested by Marchioli,[27] Bassenne *et al.*,[28] and Johnson *et al.*[29]

This paper proposes a coupling strategy to improve the behavior of existing advanced static models when used in a WMLES context. Main ideas for this work come from stochastic forcing methods as proposed in Mason and Thomson,[30] Piomelli *et al.*,[31] or Keating and Piomelli.[32] Their original purposes were however in the context of Reynolds-averaged Navier–Stokes (RANS)/LES boundary layer modeling to represent backscatter or to decrease the transition region between the RANS and LES zones. The goal is here different and is to generate stochastic fluctuations of velocity gradients that feed the SGS models, as a correction for the incompatibility between SGS models with the proper near-wall asymptotics and the WMLES framework.

The paper is organized as follows. In Sec. II, the methodology including the test case and the numerics is described. A brief comparative study between Smagorinsky, WALE, and Sigma models is then proposed to illustrate the identified weaknesses of the default coupling strategy. In Sec. III, the development of a dedicated stochastic forcing is introduced and applied to the different SGS models and results are discussed. Finally, Sec. IV concludes and provides some perspectives.

II. PRESENTATION OF THE PROBLEM

A. Numerical framework

The LES code AVBP developed by CERFACS[33–35] is used in this study. In its original form, it solves the compressible Navier–Stokes equations for unstructured meshes with a finite volume cell-vertex formalism. Although mainly dedicated to compressible applications such as combustion, the code has been validated in incompressible framework such as two-phase flow problems[36,37] and is therefore adapted for the present work dealing with incompressible test cases (Sec. II B). A Lax-Wendroff[38] (second order in space and time) numerical scheme coupled to a third-order Runge–Kutta procedure for time advancement is applied. The filtered equations for mass, momentum, and energy are written below:

$$\frac{\partial \bar{\rho}}{\partial t} + \frac{\partial \bar{\rho}\widetilde{u}_i}{\partial x_i} = 0, \tag{1}$$

$$\frac{\partial \bar{\rho}\widetilde{u}_j}{\partial t} + \frac{\partial \bar{\rho}\widetilde{u}_i\widetilde{u}_j}{\partial x_i} + \frac{\partial \bar{P}\delta_{ij}}{\partial x_i} = \frac{\partial}{\partial x_i}\left[\bar{\tau}_{ij} - \bar{\rho}\left(\widetilde{u_i u_j} - \widetilde{u}_i\widetilde{u}_j\right)\right], \tag{2}$$

$$\frac{\partial \bar{\rho}\widetilde{E}}{\partial t} + \frac{\partial \bar{\rho}\widetilde{u}_i\widetilde{E}}{\partial x_i} + \frac{\overline{\partial u_i P\delta_{ij}}}{\partial x_i} = \frac{\partial}{\partial x_i}\left[\overline{q_i} - \bar{\rho}\left(\widetilde{u_i E} - \widetilde{u}_i\widetilde{E}\right)\right] + \overline{\tau_{ij}\frac{\partial u_i}{\partial x_j}}, \tag{3}$$

where ρ is the mixture density, u_i stands for the ith component of the velocity, P the pressure, τ_{ij} the viscous stress tensor, E the total non-chemical energy, q_i the ith component of the heat flux, and δ_{ij} is the Kronecker symbol, equal to 1 if $i=j$ and 0 otherwise. In these notations, the operator $\bar{\cdot}$ represents a Reynolds-filtered variable and the operator $\widetilde{\cdot}$ denotes the mass-weighted Favre averaging.

The term $\bar{\tau}_{ij}^{sgs} = -\bar{\rho}(\widetilde{u_i u_j} - \widetilde{u}_i\widetilde{u}_j)$ is the sub-grid scale viscous stress tensor and is modeled following the Boussinesq assumption, where the subgrid stresses are modeled thanks to a subgrid scale viscosity $\nu_t = \mu_t/\rho$ (with the hypothesis of having only a dissipative role on the larger structures),

$$\bar{\tau}_{ij}^{sgs} = 2\bar{\rho}\nu_t\left(\widetilde{S}_{ij} + \frac{1}{3}\delta_{ij}\widetilde{S}_{ll}\right), \tag{4}$$

where

$$\widetilde{S}_{ij} = \frac{1}{2}\left(\frac{\partial \widetilde{u}_j}{\partial x_i} + \frac{\partial \widetilde{u}_i}{\partial x_j}\right). \tag{5}$$

The turbulent viscosity ν_t is computed depending on the chosen subgrid scale model, being in this paper Smagorinsky,[19] WALE,[20] or Sigma.[21]

Since the overall context of work is WMLES, wall modeling has to be introduced to complement the above equations in the near-wall region. Variables expressed in wall units (superscript "+") are useful

to express a unified vision of the turbulent boundary layer. Based on the friction velocity u_τ and the viscous length scale δ_ν, the wall distance and the velocity are normalized as

$$y^+ = \frac{y}{\delta_\nu} = \frac{\rho_w u_\tau y}{\mu_w}, \quad u^+ = \frac{u}{u_\tau}, \tag{6}$$

where the subscript "w" stands for wall values (in the cell-vertex formalism, variables are stored at nodes). The classic two-layer logarithmic law distinguishes the viscous sub-layer from the log-layer with $y_c^+ = 11.445$ as the cutoff value so that

$$u^+ = \frac{1}{\kappa}\ln\left(y^+\right) + C \text{ if } y^+ > y_c^+, \tag{7}$$

$$u^+ = y^+ \text{ otherwise}, \tag{8}$$

where $\kappa = 0.41$ is the Von Kármán constant and $C = 5.5$ for internal flows. Note that this classic wall law is used in this work in a local and instantaneous way, even though it has been originally developed for RANS;[9] however, it has been commonly used in LES as well. More advanced wall laws exist but are not considered in this work as the classic wall law is still largely used in industrial LES that is the target of this study, and the cases described further fit the assumptions made for the derivation of the classic wall law.

The friction flux is computed as

$$\tau_w = \rho_w u_\tau^2, \tag{9}$$

with

$$u_\tau = \sqrt{(u_1\mu_w)/(y_1\rho_w)}, \tag{10}$$

where the subscript "1" indicates the first off-wall node value (cf. Fig. 1).

From the friction flux predicted by the wall law and imposed as a Neumann boundary condition, the wall velocity gradient is expressed as

$$\left.\frac{\partial u}{\partial y}\right|_{w,wall-law} = \frac{\tau_w}{\mu_w + \mu_{t,w}}, \tag{11}$$

with $\mu_{t,w}$ the wall turbulent dynamic viscosity. Equation (11) leads to a non-zero slip velocity u_{slip} as illustrated in Fig. 1. This is actually where the coupling between the wall law and the sub-grid scale model appears: At the next iteration, u_{slip} (which is unphysical but still results from the convective scheme) and u_1 are used to compute the wall velocity gradient that feeds the SGS model. Then, μ_t acts directly on the next evaluation of the exact wall velocity gradient through Eq. (11): high values of μ_t will lead to a moderate velocity gradient, while low values of μ_t induce steep wall velocity gradient, as observed in Jaegle *et al.*[22] and can lead to reversed slip velocities and spurious oscillations.

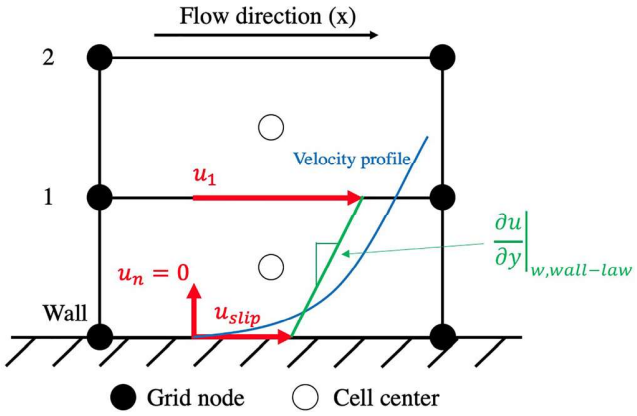

FIG. 1. Near-wall velocities scheme.

B. Numerical setup

The simple bi-periodic turbulent channel flow configuration[39] of half-height h as sketched in Fig. 2 is used hereafter to illustrate the issue and test the coupling strategy. In this specific case, the problem is statistically steady and the average flow can be considered one-dimensional, meaning that $\partial/\partial t = 0$, $\partial/\partial x = 0$, $\partial/\partial z = 0$. Under these conditions, the momentum equation, Eq. (2), reduces to

$$\frac{\partial}{\partial y}\left(\overline{\mu\frac{\partial u}{\partial y}} - \bar{\rho}\widetilde{u''v''} + \overline{\mu_t\frac{\partial u}{\partial y}}\right) = -S_x, \tag{12}$$

where $\bar{\rho}\widetilde{u''v''}$ is the LES resolved turbulence contribution and S_x is a source term needed to equilibrate the wall shear as the mean pressure gradient is zero due to periodicity. This source term can be evaluated using the Kármán–Nikuradse correlation[40] (abbreviated "KNc" hereafter) that predicts a friction coefficient $C_{f,KNc}$, based on the bulk Reynolds number and hydraulic diameter $Re_{b,Dh}$,

$$C_{f,KNc} = 0.046\, Re_{b,Dh}^{-0.2}, \tag{13}$$

$$\tau_{w,KNc} = 0.5\, C_{f,KNc}\, \rho u^2. \tag{14}$$

This source term is imposed dynamically to maintain the target mass flow rate (or equivalently, the bulk Reynolds number),

$$S_x^{t+\Delta t} = \frac{(\rho u)_{\text{target}} - \frac{1}{V}\int\int\int_\Omega (\rho u)^t dV}{\tau_{\text{relax}}}, \tag{15}$$

where t denotes the current time step, Δt is the computational time step, V is the integration volume in the domain Ω, and τ_{relax} is a relaxation time coefficient, taken to $\tau_{relax} = 1/3 \times h/u_\tau$ in this study.

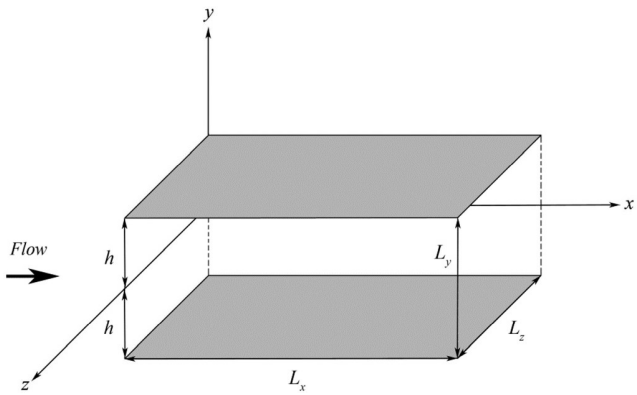

FIG. 2. Turbulent channel geometry. Gray surfaces represent wall boundary conditions (making use of the wall law), while the other pairs of faces are periodic.

Following the DNS of Hoyas and Jimenez,[41] two cases are considered at $Re_\tau = 547$ and $Re_\tau = 934$ (with $Re_\tau = u_\tau h/\nu_w$), as test cases for analyzing and developing the wall-law/SGS model coupling strategy. The WMLES cases are built with meshes, respectively, satisfying $y^+ \approx 55$ and $y^+ \approx 95$, ensuring that the wall nodes are in the log zone of the boundary layer. Note that for these cases, meshes are regular and fully made of hexaedra (of dimensions $\Delta x^+, \Delta y^+, \Delta z^+$), while the channels have the same dimensions as indicated by Hoyas and Jimenez[41] (cf. Table I for mesh characteristics).

To finish, although the solver is fully compressible, the operating mean flow pressure is fixed at 1 MPa so that $M < 0.05$ in both cases, ensuring that no compressible effect is present. The wall boundary condition relies on a slip formalism ($u_n = 0$ with a slip velocity $u_{slip} \neq 0$, cf. Fig. 1 and Jaegle *et al.*[22] for the implementation) and the standard law of the wall, used with an isothermal condition that is also the flow temperature. The flow is thus virtually isothermal, and the interest is put on the viscous flux of momentum through the solid wall: the wall shear stress. Also, the heat generated by viscous dissipation is clearly negligible given the Mach number considered. As a consequence, density and viscosity are nearly constant in the whole channel.

All simulations are performed with the Smagorinsky, WALE, and Sigma models and are time-averaged over at least 100 diffusive times ($100 \times h/u_\tau$) to ensure statistical convergence.

C. Comparison between SGS models for wall shear stress prediction

The wall shear stress obtained by using the different SGS models within the WMLES framework described in Sec. II A are displayed in Tables II and III. Although the following focuses on case $Re_\tau = 547$, the comments are valid for the case $Re_\tau = 934$. In the results presented below, the friction flux computed with the Kármán–Nikuradse correlation ("KNc"), Eq. (14), is taken as the reference. Note that the incompressible nature of the simulations has been checked following the Morkovin hypothesis that has been verified in past studies,[42,43] stating that the compressibility effects on turbulent statistics are limited to the mean density variations (here below 0.003% in space and time) as long as the fluctuating Mach number is small.

The results clearly show that the Sigma and WALE models fail to accurately predict the wall shear stress in this WMLES context, with about $\approx +20\%$ and $\approx +25\%$ for $Re_\tau = 547$, and $\approx +22\%$ and $\approx +28\%$ errors, respectively, for $Re_\tau = 934$ for the friction flux. Contrarily, the Smagorinsky model gives a good prediction by providing an error of only $\approx +3$–4%. Such differences can be effectively related to the fact that u_τ is over-predicted with Sigma and WALE, the first off-wall velocity u_1 being clearly overestimated with these models as observed from Fig. 3(a) contrarily to the Smagorinsky SGS closure. This specific overestimation of τ_w then expresses in reduced slopes of the log-law velocity profiles as shown by Fig. 3(b) for Sigma and WALE.

The over-prediction of the effective turbulent Reynolds number and wall friction can be explained as follows. Since all SGS models are gradient diffusion-based models making use of a turbulent viscosity, their physical action is purely dissipative when it comes to energy and purely diffusive when it comes to momentum. However, by construction Sigma and WALE provide a turbulent viscosity that is linked to the near-wall velocity gradient, which itself depends on the wall distance. The near-wall velocity gradient being under-resolved and the near-wall velocity fluctuation being too weak, and it results a streamwise off-wall velocity value u_1 that is overestimated compared to what it should be. Indeed, its coupling with the wall law relying on Eq. (10), an overestimation of $\tau_w = \rho_w u_\tau^2$, is found as reported by Tables II and III. Note that in such a scheme, a good prediction of τ_w requires a good first off-wall streamwise velocity u_1 estimation (like in the Smagorinsky case) or conversely a good turbulent SGS viscosity and velocity gradient. This last critical issue is of particular importance as emphasized in Sec. III.

In a wall-resolved context, the Smagorinsky model is known to induce overestimated turbulent viscosity in the near-wall region, because of its response to the wall shear stress. To address this issue, WALE and Sigma have been developed to induce a turbulent viscosity that follows a y^3 damping when approaching the wall. This intends to comply with the wall-resolved physics,[44] where no turbulent activity exists in the viscous sub-layer. However, in a WMLES context, this y^3 damping function is no longer relevant since the first off-wall node is located in the logarithmic region, which contains turbulent activity. Still, Fig. 3(d) shows that this asymptotic behavior also occurs in WMLES, meaning that it is independent of the y^+ or τ_w values.

Figure 3(a) shows that the choice of SGS model also affects the wall slip velocity: $u_{slip} \approx 5.8\,\mathrm{m/s}$ using a Smagorinsky model, while $u_{slip} \approx 1.6\,\mathrm{m/s}$ with WALE of Sigma. Although unphysical and artificially resulting from the law of the wall implementation,[22] this wall velocity impacts the code evaluation of the normal streamwise velocity gradient that then propagates to the near-wall nodes through the diffusion process (either SGS or laminar process) as shown in Fig. 3(c). A direct consequence of the small slip velocity produced by WALE of

TABLE I. Meshes used for the channel flow test cases considered.

Case	Re_b	L_x/h	L_z/h	$N_x \times N_y \times N_z$	Δx^+	Δy^+	Δz^+
Re_τ 547	10450	$8\,\pi$	$4\,\pi$	$201 \times 21 \times 101$	69	55	69
Re_τ 934	18950	$8\,\pi$	$3\,\pi$	$201 \times 21 \times 101$	117	95	88

TABLE II. Comparison of the wall shear stress in the turbulent channel flow for $Re_\tau = 547$. Errors are relative to the KNc.

	KNc	Smagorinsky		Sigma		WALE	
	Value	Value	Error	Value	Error	Value	Error
τ_w (Pa)	2.59	2.69	+3.77%	3.11	+19.97%	3.24	+24.98%

TABLE III. Comparison of the wall shear stress in the turbulent channel flow for $Re_\tau = 934$. Errors are relative to the KNc.

	KNc	Smagorinsky		Sigma		WALE	
	Value	Value	Error	Value	Error	Value	Error
τ_w (Pa)	7.57	7.82	+3.33%	9.22	+21.83%	9.70	+28.17%

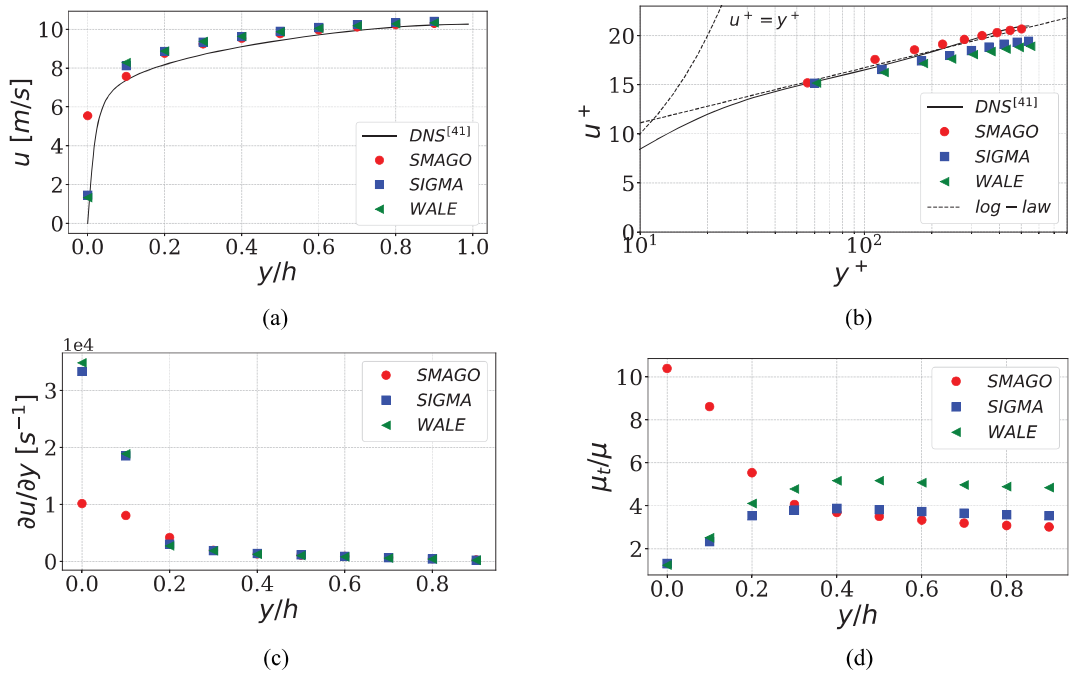

FIG. 3. Comparison between the different SGS models for the channel flow $Re_\tau = 547$. (a) Streamwise velocity. (b) Streamwise velocity in wall units. (c) Streamwise velocity gradient. (d) Dynamic viscosity ratio.

Sigma is to generate higher velocity gradients than Smagorinsky at the first two nodes.

The limitations of WMLES and more specifically the coupling scheme adopted between the law of the wall and any SGS model have been evidenced. WALE and Sigma near-wall behavior is physically justified in WRLES, but fails to characterize the near-wall region in WMLES where the first off-wall node lies in the logarithmic region. Contrarily, although the Smagorinsky model is known, in a wall-resolved context, to have physical limitations especially in sheared flows, its coupling with a law of the wall appears satisfying in the WMLES context. Because these SGS models rely on the filtered velocity gradient, which is wrong in the framework of WMLES, the choice of the SGS model in a WMLES context may significantly impact the wall shear stress prediction.

III. PROPOSED WMLES/SGS COUPLING FRAMEWORK

The problem of WMLES and the coupling with different SGS models has been evidenced in the specific cases of the Smagorinsky, WALE, and Sigma models. The following discussion therefore proposes a correction framework to facilitate the coupling between a law of the wall and WALE or Sigma models while guaranteeing robust near-wall flow predictions. The idea followed in this paper is to artificially generate the missing turbulent activity in the first cell of the wall-modeled mesh, so that the velocity gradients feeding these SGS models would be representative of the actual physics. Indeed, SGS models build the turbulent viscosity operator with the assumption of a turbulent physical property, generally presuming a velocity gradient of the resolved field sufficiently representative of the true SGS turbulent activity. Adding fluctuations to the velocity gradients of the resolved field can therefore help meeting initial goal that is to manipulate a locally turbulent field, which is not guaranteed if a law of the wall is used.

The general idea of the proposed approach is therefore to keep the WALE and Sigma models untouched in the bulk flow while modifying the velocity gradients in the near-wall region. The goal is to recover a corrected turbulent viscosity value in this region of the flow to ensure an accurate wall shear stress prediction.

A. Development of the stochastic forcing approach

This subsection intends to relate the expected velocity gradient near-wall activity to the available LES variables. To reach this objective, a Reynolds-averaged Navier–Stokes approach, for which the logarithmic region is valid, is followed in a first step. This first step evaluates the expected turbulent kinetic energy within the first cell, on the basis of the filtered LES quantities within the outer layer. This turbulent kinetic energy is then recast in terms of fluctuating velocity gradients and complies with the unsteady LES context. This fluctuating velocity gradients are finally generated using a stochastic approach and added within the first LES cell to correct the predicted velocity gradient, to account for the missing turbulent activity.

In order to relate the turbulent kinetic energy with the external LES velocity, both a mixing-length algebraic model and a turbulent kinetic energy model[45] are used. On one hand, the mixing-length algebraic model writes

$$\nu_t = l_m^2 \frac{\partial u}{\partial y}, \tag{16}$$

where l_m is the mixing length.[46] It can be shown that in the overlap region ($50\delta_v < y < 0.1\delta$), as well in the log region, the mixing length writes[47]

$$l_m = \kappa y, \tag{17}$$

where κ is the von Kármán constant. Furthermore at high Reynolds number, within the log-zone,[45]

$$\frac{\partial u}{\partial y} = \frac{u_\tau}{\kappa y}. \tag{18}$$

The mixing-length model can therefore be recast into

$$\nu_t = u_\tau \kappa y. \tag{19}$$

On the other hand, the turbulent kinetic energy evolution model[45] follows:

$$\nu_t = C_\mu^{1/4}\sqrt{k} l_m, \text{ with } C_\mu = 0.09, \tag{20}$$

where k stands for the turbulent kinetic energy. Hence, combining Eqs. (16), (18), and (20), one gets across the log-region,

$$\nu_t = C_\mu^{1/4}\sqrt{k} l_m = l_m^2 \frac{u_\tau}{\kappa y}. \tag{21}$$

Injecting Eq. (17) into Eq. (21) allows to establish

$$C_\mu^{1/4}\sqrt{k} = u_\tau, \tag{22}$$

so that the kinetic energy within the log region finally writes

$$k = \frac{u_\tau^2}{\sqrt{C_\mu}} = \frac{\tau_w}{\rho_w \sqrt{C_\mu}}. \tag{23}$$

Note that this last expression provides an evaluation of the local turbulent kinetic energy based on the wall variables τ_w and ρ_w.

The next step is to evaluate the velocity gradient activity: the turbulent kinetic energy dissipation rate ε within the log law framework is used.[45] Using Eq. (19), one can write

$$\varepsilon = \frac{C_\mu k^2}{\nu_t} = \frac{C_\mu k^2}{u_\tau \kappa y}, \tag{24}$$

or, using the wall units $y^+ = y/\delta_v$ and $\delta_v = \nu_w/u_\tau$,

$$\varepsilon = \frac{C_\mu k^2}{u_\tau \kappa y^+ \delta_v} = \frac{C_\mu k^2}{\kappa y^+ \nu_w}. \tag{25}$$

The assumption of homogeneous isotropic turbulence (HIT) is now called upon. Although it might appear as a strong assumption considering wall-bounded flows, Schlichting[48] argued that even if strictly speaking isotropic turbulence does not exist in nature, Eq. (26) hereafter enjoys a very wide applicability if one considers locally isotropic turbulence, that is, large gradients of the fluctuating velocity field ($\partial u_i'/\partial x_j$), which is exactly the context adopted here. With this assumption, Taylor[49] demonstrated that

$$\varepsilon = 15\nu\overline{\left(\frac{\partial u'}{\partial x}\right)^2}, \tag{26}$$

where u' denotes the turbulent velocity fluctuation.

Using Eqs. (25) and (26), the gradient of the fluctuating velocity follows:

$$\overline{\left(\frac{\partial u'}{\partial x}\right)^2} = \frac{C_\mu k^2}{15\kappa y^+ \nu_w^2}. \tag{27}$$

Then using Eq. (23) to substitute the turbulent kinetic energy, one finally gets

$$\overline{\left(\frac{\partial u'}{\partial x}\right)^2} = \frac{C_\mu \tau_w^2}{15\nu_w^2 \kappa y^+ \rho_w^2 C_\mu} = \frac{\tau_w^2}{15\kappa y^+ \mu_w^2}. \tag{28}$$

With the HIT assumption, Taylor also demonstrated that

$$\overline{\left(\frac{\partial u'}{\partial x}\right)^2} = \frac{1}{2}\overline{\left(\frac{\partial u'}{\partial y}\right)^2} = \frac{1}{2}\overline{\left(\frac{\partial u'}{\partial z}\right)^2}, \tag{29}$$

$$\overline{\left(\frac{\partial u'}{\partial x}\right)^2} = \overline{\left(\frac{\partial v'}{\partial y}\right)^2} = \overline{\left(\frac{\partial w'}{\partial z}\right)^2}, \tag{30}$$

which leads to the root mean square quantities,

$$\sqrt{\overline{\left(\frac{\partial u_i'}{\partial x_j}\right)^2}} = \frac{\tau_w}{\sqrt{15\kappa y^+}\mu_w} \quad \text{for i = j}, \tag{31}$$

and

$$\sqrt{\overline{\left(\frac{\partial u_i'}{\partial x_j}\right)^2}} = \sqrt{2}\frac{\tau_w}{\sqrt{15\kappa y^+}\mu_w} \quad \text{for i} \neq j. \tag{32}$$

Finally, to reconstruct LES-filtered values, a random variable is introduced that is arbitrary chosen to follow a normal distribution to represent these fluctuations. The quantile function (also known as the inverse cumulative distribution function) of a normal distribution writes

$$f(\zeta) = \gamma + \sigma\sqrt{2} erf^{-1}(2\zeta - 1), \tag{33}$$

γ being the mean, considered here as the initial prediction of the LES code, and σ is the standard deviation. ζ is a random variable with $0 \leq \zeta \leq 1$. σ being computed from Eqs. (31) and (32), this leads to

$$\left(\frac{\partial u_i'}{\partial x_j}\right)(\zeta) = \frac{\tau_w}{\sqrt{15\kappa y^+}\mu_w}\sqrt{2} erf^{-1}(2\zeta - 1) \quad \text{for i = j}, \tag{34}$$

and

$$\left(\frac{\partial u_i'}{\partial x_j}\right)(\zeta) = \frac{\tau_w}{\sqrt{15\kappa y^+}\mu_w} 2 erf^{-1}(2\zeta - 1) \quad \text{for i} \neq j. \tag{35}$$

Ultimately, the velocity gradient tensor used in the turbulent viscosity operator of WALE or Sigma models is corrected as

$$\left(\frac{\partial \widetilde{u}_i}{\partial x_j}\right)_{corr} = \left(\frac{\partial \widetilde{u}_i}{\partial x_j}\right)_{LES} + \left(\frac{\partial u_i'}{\partial x_j}\right)(\zeta). \tag{36}$$

In the specific cell-vertex context of AVBP, the correction is applied at the cell center of the wall cells as described in Fig. 4. Note that ζ is

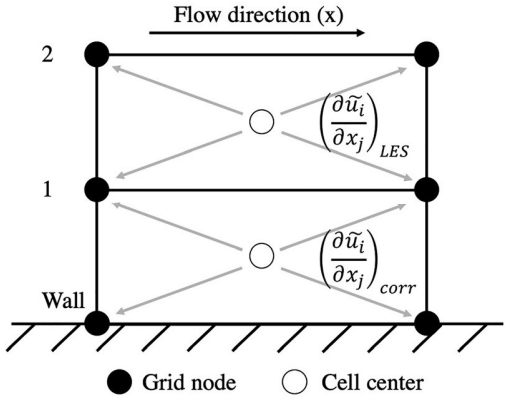

FIG. 4. Velocity gradient modification at the wall: artificial fluctuations are generated at the wall cell center. The corrected velocity gradient then feeds the SGS operator also computed at the cell center. The resulting turbulent viscosity is then scattered at the wall and off-wall nodes. The rest of the domain is not modified.

randomly generated for each gradient component at each node and at each integration time step. For each concerned wall cell, nine gradients (in 3 D) are therefore perturbed as described above. Finally, a particular emphasis is put on this point: the fluctuations are only used to build the turbulent viscosity value and are not used elsewhere in the code (*i.e.*, the velocity field is not changed directly, and its modification is only induced by the modified μ_t value).

The resulting WMLES framework, coupling the law of the wall, the SGS model, and the proposed stochastic forcing method, is summarized in Fig. 5.

B. Results with stochastic forcing

In the following, the proposed coupling formalism is applied to the previous test cases using WALE and Sigma, respectively, denoted by the "_sf" tag (for "*stochastic forcing*") to distinguish them with the non-perturbed wall velocity gradient cases. Note that with the use of the proposed strategy, the computational speed of the simulations has been decreased by about 2%.

Wall shear stress issued by the new proposed coupling for the $Re_\tau = 547$ and $Re_\tau = 934$ cases are presented in Tables IV and V. They evidence a significant improvement in τ_w predictions for WALE and Sigma with the proposed stochastic forcing. The prediction errors are reduced from $\simeq$25% to about 4% for WALE, and from $\simeq$20% to about 1% for Sigma.

Figures 6(a) and 6(b) illustrate velocity profiles for Sigma and WALE with the proposed stochastic forcing that are found in close agreement with the one obtained with the Smagorinsky model, without the gradient perturbations. The first off-wall velocity value is found to be exactly on the DNS prediction. This is confirmed by the profiles plotted in wall units, Figs. 6(c) and 6(d), evidencing that the proposed correction has significantly reduced the previously obtained log-layer mismatch. As pointed out in Sec. II B, this specific point is at the origin of the observed improvement since this velocity is related to u_τ and therefore τ_w.

The impact of the proposed correction on the turbulent viscosity profiles is observed on Figs. 6(e) and 6(f). Trends are now reversed, Sigma and WALE providing more turbulent viscosity in the near-wall region as expected in a WMLES context. This is also highlighted on Fig. 7 depicting instantaneous fields of wall turbulent viscosity for Smagorinsky, Sigma, and corrected Sigma models, where the effect of added fluctuations is clearly visible at the wall. The direct consequence of the proposed forcing is to increase dissipation at the wall, as shown by Fig. 8. As anticipated, the added fluctuations fulfill their role although the limit of the proposed approach can be a too dissipative/diffusive process. Although dissipation is usually considered as a drawback for LES, it allows here to enhance the wall shear stress prediction, to provide a better modeling of the turbulent structures enclosed within the first cell in the WMLES context. Therefore, a better

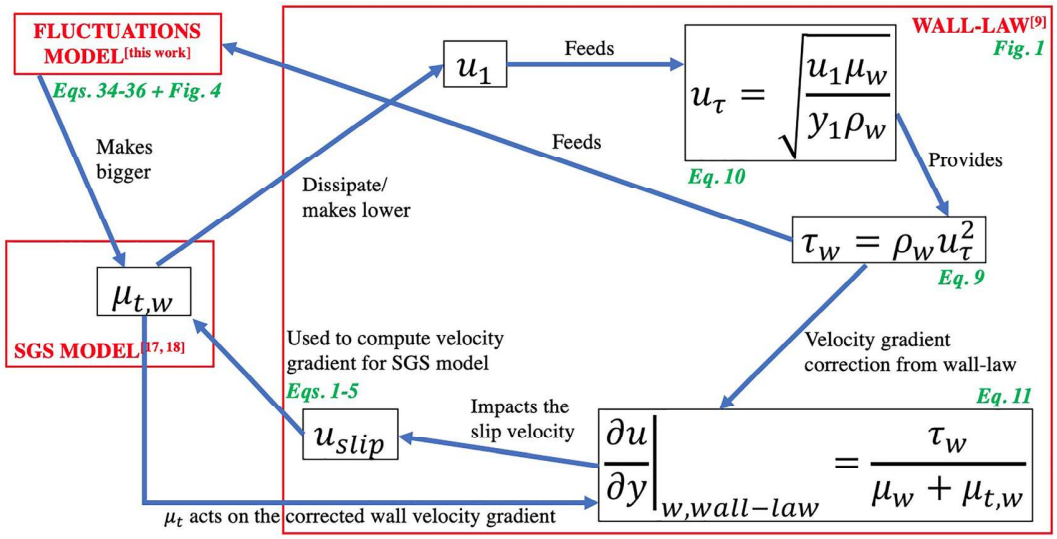

FIG. 5. Sum up of the coupling strategy between the wall law, SGS model, and the proposed fluctuations model/stochastic forcing.

TABLE IV. Comparison of the wall shear stress in the turbulent channel flow $Re_\tau = 547$ with stochastic forcing. Errors are relative to the KNc.

	KNc	Sigma_sf		WALE_sf	
	Value	Value	Error	Value	Error
τ_w	2.59	2.58	−0.48%	2.51	−3.18%

TABLE V. Comparison of the wall shear stress in the turbulent channel flow $Re_\tau = 934$ with stochastic forcing. Errors are relative to the KNc.

	KNc	Sigma_sf		WALE_sf	
	Value	Value	Error	Value	Error
τ_w	7.57	7.44	−1.69%	7.17	−5.26%

turbulent kinetic energy profile is found when compared to the DNS, Fig. 9: again, Smagorinsky seems to better fit the DNS due to its better original prediction of the wall shear stress, and thanks to the fluctuations WALE and Sigma tend also to match better the DNS results.

The detail of the turbulent kinetic energy can be found in the second-order moment of the statistics, namely, the root mean square ("rms") of the velocity components, which are presented in Fig. 10. They highlight a strong impact of the proposed model on the velocity fluctuations that are found closer to the Smagorinsky case and way more in accordance with the DNS for the streamwise direction [Figs. 10(a) and 10(b)]. For the other directions [wall-normal and spanwise, Figs. 10(c)–10(f)], the comparison with the DNS is not as straightforward: the near-wall zone (until $y^+ = 200$) seems in favor of the non-model cases for both Sigma and WALE, but in the channel bulk flow ($y^+ > 200$), the agreement is overall better with the model. Note a particular behavior due to the coupling effect of the strategy: even if

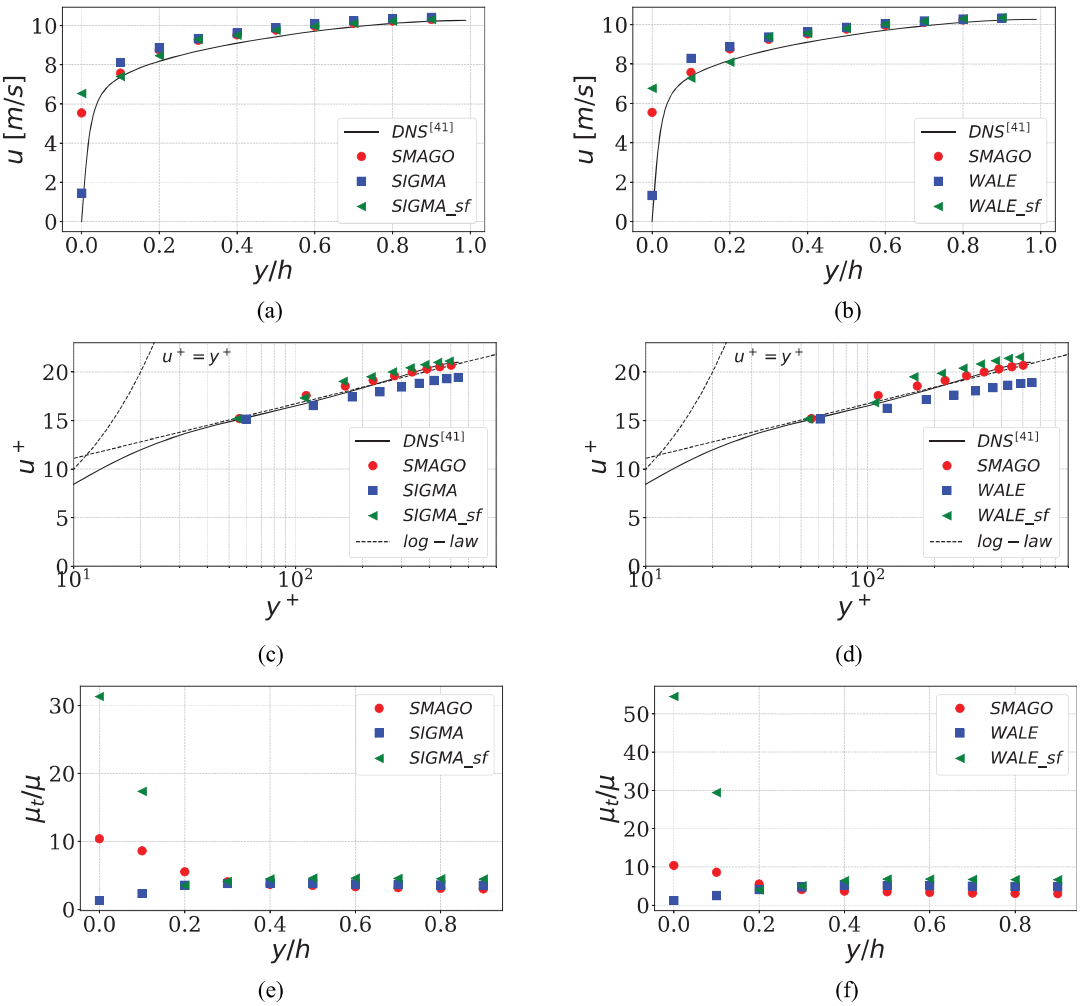

FIG. 6. Comparison between the SGS models with adding of the gradients of velocity fluctuations for channel flow $Re_\tau = 547$. (a) Streamwise velocity, Sigma. (b) Streamwise velocity, WALE. (c) Streamwise velocity in wall units, Sigma. (d) Streamwise velocity in wall units, WALE. (e) Dynamic viscosity ratio, Sigma. (f) Dynamic viscosity ratio, WALE.

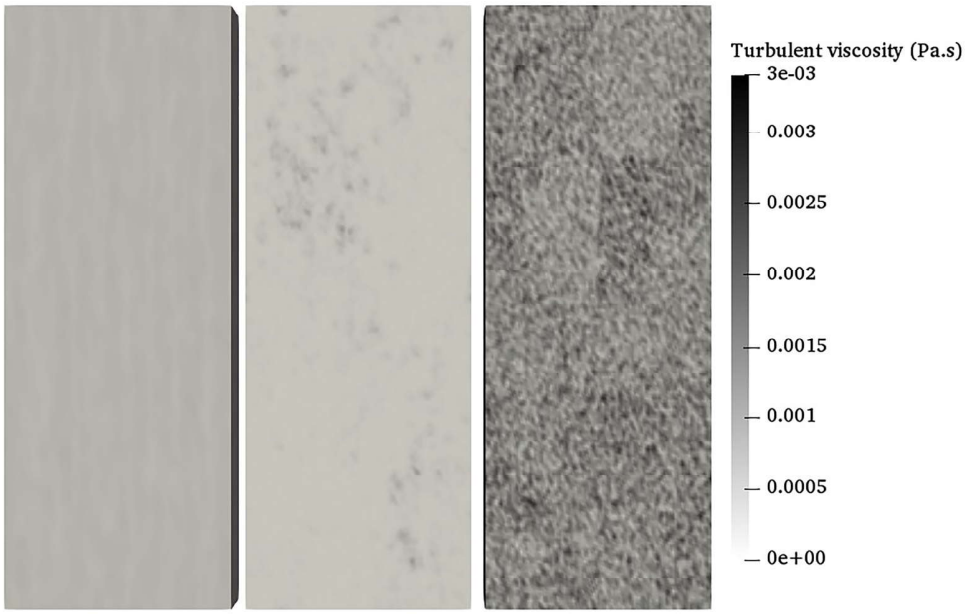

FIG. 7. Instantaneous fields of the wall turbulent viscosity ($\mu_{t,w}$), in the case $Re_\tau = 934$. From left to the right: Smagorinsky, Sigma, and Sigma with fluctuations.

fluctuations of velocity gradients are added, as their effect is to increase the wall turbulent viscosity, which leads to a better estimation of the wall friction flux that was initially over-estimated, the rms are actually lower with the use of the model than without.

Note that the proposed method relies on the generation of random fluctuations of velocity gradients, but one could also choose to directly act on the fluctuating velocity (therefore at a node level instead of the cell level for the specific cell-vertex context of AVBP). Following

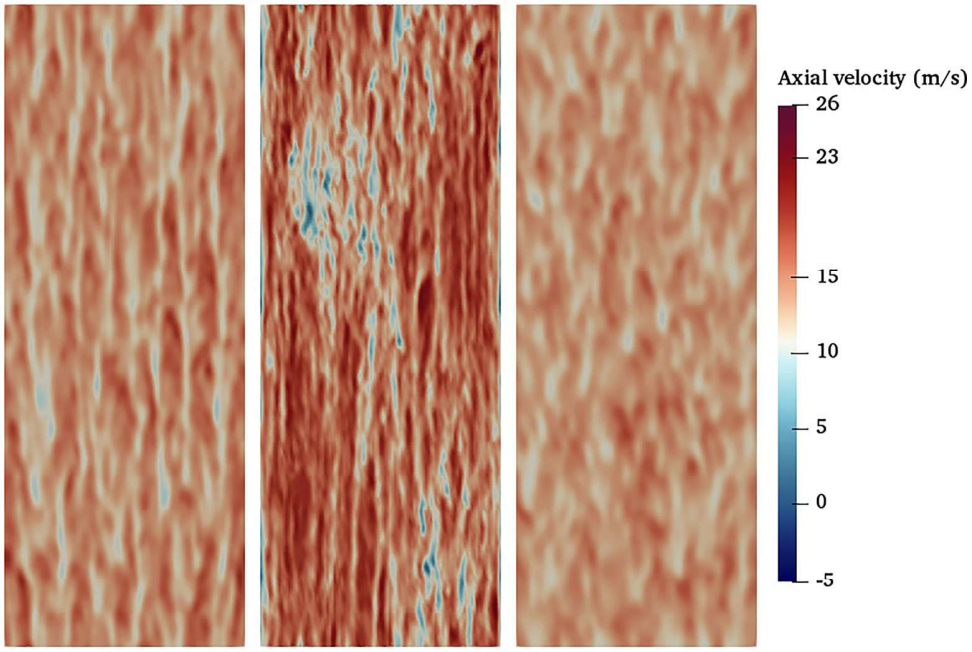

FIG. 8. Instantaneous fields of the first off-wall axial velocity (u_1), in the case $Re_\tau = 934$. From left to the right: Smagorinsky, Sigma, and Sigma with fluctuations.

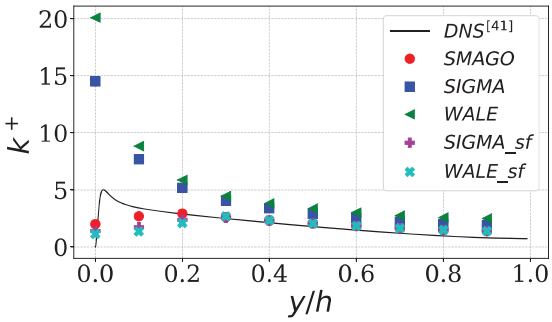

FIG. 9. Turbulent kinetic energy (in wall units) for all the models for the case $Re_\tau = 934$.

similar developments as the one presented in Sec. III A, a relation between the turbulent kinetic energy and velocity fluctuations can be established using a correlation coefficient of the form $u_i'^2/k = C_i$ within the log-layer, C_i being constants provided in Pope[45] for example. Although not detailed here, similar results were obtained for both the velocity profiles and the wall shear stress predictions with this second approach. However, a tuning process of the velocity fluctuating intensity at the wall nodes was found necessary, which is therefore case-dependent and not relevant for general consideration.

IV. CONCLUSION

A stochastic forcing method is proposed in this paper to address the log-layer mismatch experienced through the use of WALE and Sigma subgrid scale models in a wall-modeled LES context (WMLES).

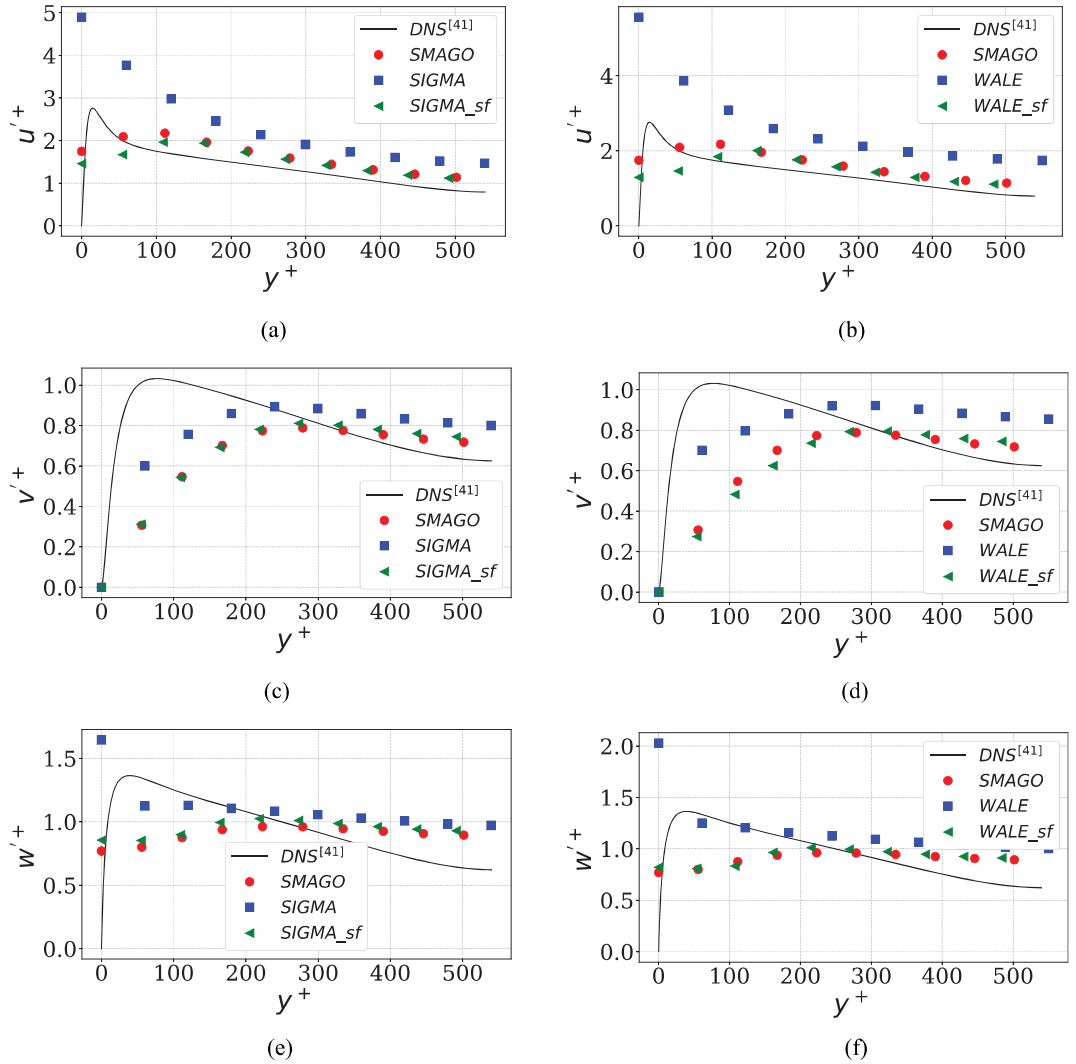

FIG. 10. Comparison between the SGS models of the root mean square of the velocity components with adding of the gradients of velocity fluctuations for channel flow $Re_\tau = 547$, in wall units. (a) Streamwise rms velocity, Sigma. (b) Streamwise rms velocity, WALE. (c) Wall-normal rms velocity, Sigma. (d) Wall-normal rms velocity, WALE. (e) Spanwise rms velocity, Sigma. (f) Spanwise rms velocity, WALE.

Results with a classical use of Smagorinky, WALE, and Sigma on a WMLES turbulent channel configuration are first investigated, and evidence accurate wall predictions with Smagorinsky (known to be too dissipative in the bulk flow), while the WALE and Sigma models predict an overestimated wall shear stress with about 25% of error. It is shown that this behavior results from the inherent turbulent viscosity damping at the wall with the WALE and Sigma models, that is, an accurate behavior in a wall-resolved context, but not in a wall-modeled one where the first off-wall node lies in the logarithmic region. Such turbulent viscosity damping does not allow one to model the turbulent structures within the first cell.

To address this indirect weakness, a combination of the mixing-length algebraic model and the turbulent kinetic energy model is considered to provide the expected kinetic energy within the log region on the basis of the available LES quantities at the wall and first off-wall node. This evaluated turbulent kinetic energy is then recast in terms of unsteady LES quantities through a stochastic forcing that provides a gradient of fluctuating velocity within the first cell. This stochastic forcing allows to correct the gradient predicted by the law of the wall and accurately feeds the WALE and Sigma operators thus accounting for turbulent activity within the first cell.

Results show that this stochastic forcing procedure allows to reduce the log-layer mismatch with WALE and Sigma SGS models in a WMLES context, and error predictions for the wall shear stress are reduced from $\simeq$25% to about 4% for WALE and from $\simeq$20% to about 1% for Sigma.

Future work will be devoted to anisothermal channels with high temperature gradients between the wall and the bulk flow, which suffer from similar issues in WMLES, and focus will be put on the wall heat flux prediction.

ACKNOWLEDGMENTS

This work has been funded by CNES and ArianeGroup and was performed using HPC resources from GENCI-[TTGC] (Grant No. 2021-A0092B10157).

The authors have no conflicts to disclose.

DATA AVAILABILITY

The data that support the findings of this study are available within the article.

REFERENCES

[1]M. Germano, "Turbulence—The filtering approach," J. Fluid Mech. **238**, 325–336 (1992).
[2]A. Kolmogorov, "The local structure of turbulence in incompressible viscous fluid for very large Reynolds numbers," Proc. R. Soc. London Ser. A **434**, 9–13 (1941); available at https://www.jstor.org/stable/51980?origin=JSTOR-pdf.
[3]P. Sagaut, *Large Eddy Simulation for Incompressible Flows* (Springer, 2006).
[4]M. Lesieur, *Turbulence in Fluids*, 4th ed. (Springer, 2008).
[5]D. R. Chapman, "Computational aerodynamics development and outlook," AIAA J. **17**, 1293–1313 (1979).
[6]H. Choi and P. Moin, "Grid-point requirements for large eddy simulation: Chapman's estimates revisited," Phys. Fluids **24**, 011702 (2012).
[7]J. Larsson, S. Kawai, J. Bodart, and I. Bermejo-Moreno, "Large eddy simulation with modeled wall-stress: Recent progress and future directions," Mech. Eng. Rev. **3**, 15-00418 (2016).
[8]S. T. Bose and G. I. Park, "Wall-modeled large-eddy simulation for complex turbulent flows," Annu. Rev. Fluid Mech. **50**, 535–561 (2018).
[9]B. E. Launder and D. B. Spalding, "The numerical computation of turbulent flows," Comput. Methods Appl. Mech. Eng. **3**, 269–289 (1974).
[10]F. Nicoud, J. S. Baggett, P. Moin, and W. Cabot, "Large eddy simulation wall-modeling based on suboptimal control theory and linear stochastic estimation," Phys. Fluids **13**, 2968 (2001).
[11]S. Rezaeiravesh, T. Mukha, and M. Liefvendahl, "Systematic study of accuracy of wall-modeled large eddy simulation using uncertainty quantification techniques," Comput. Fluids **185**, 34–58 (2019), arXiv:1810.05213.
[12]H. J. Bae, A. Lozano-Durán, S. T. Bose, and P. Moin, "Dynamic slip wall model for large-eddy simulation," J. Fluid Mech. **859**, 400–432 (2019).
[13]F. De Vanna, M. Cogo, M. Bernardini, F. Picano, and E. Benini, "Unified wall-resolved and wall-modeled method for large-eddy simulations of compressible wall-bounded flows," Phys. Rev. Fluids **6**, 034614 (2021).
[14]X. I. Yang, G. I. Park, and P. Moin, "Log-layer mismatch and modeling of the fluctuating wall stress in wall-modeled large-eddy simulations," Phys. Rev. Fluids **2**, 104601 (2017).
[15]R. Deleon and I. Senocak, "The role of forcing and eddy viscosity variation on the log-layer mismatch observed in wall-modeled large-eddy simulations," J. Fluids Eng., Trans. ASME **141**, 054501 (2019).
[16]X. I. Yang and Y. Lv, "A semi-locally scaled eddy viscosity formulation for LES wall models and flows at high speeds," Theor. Comput. Fluid Dyn. **32**, 617–627 (2018).
[17]B. Giacomini and M. Giometto, "On the suitability of second-order accurate finite-volume solvers for the simulation of atmospheric boundary layer flow," Geosci. Model Dev. **14**(3), 1409–1426 (2021).
[18]H. J. Bae and A. Lozano-Durán, "Effect of wall boundary conditions on a wall-modeled large-eddy simulation in a finite-difference framework," Fluids **6**, 112–112 (2021).
[19]J. Smagorinsky, "General circulation experiments with the primitive equations," Mon. Weather Rev. **91**, 99–164 (1963).
[20]F. Nicoud and F. Ducros, "Subgrid-scale stress modelling based on the square of the velocity gradient tensor," Flow, Turbul. Combust. **62**, 183–200 (1999).
[21]F. Nicoud, H. B. Toda, O. Cabrit, S. Bose, and J. Lee, "Using singular values to build a subgrid-scale model for large eddy simulations," Phys. Fluids **23**, 085106 (2011).
[22]F. Jaegle, O. Cabrit, S. Mendez, and T. Poinsot, "Implementation methods of wall functions in cell-vertex numerical solvers," Flow, Turbul. Combust. **85**, 245–272 (2010).
[23]L. Temmerman, M. A. Leschziner, C. P. Mellen, and J. Fröhlich, "Investigation of wall-function approximations and subgrid-scale models in large eddy simulation of separated flow in a channel with streamwise periodic constrictions," Int. J. Heat Fluid Flow **24**, 157–180 (2003).
[24]P. Wu and J. Meyers, "A constraint for the subgrid-scale stresses in the logarithmic region of high Reynolds number turbulent boundary layers: A solution to the log-layer mismatch problem," Phys. Fluids **25**, 015104 (2013).
[25]S. Feng, X. Zheng, R. Hu, and P. Wang, "Large Eddy Simulation of high-reynolds-number atmospheric boundary layer flow with improved near-wall correction," Appl. Math, Mech. **41**, 33–50 (2020).
[26]S. Hickel, N. A. Adams, and N. N. Mansour, "Implicit subgrid-scale modeling for large-eddy simulation of passive-scalar mixing," Phys. Fluids **19**, 095102 (2007).
[27]C. Marchioli, "Large-eddy simulation of turbulent dispersed flows: A review of modelling approaches," Acta Mech. **228**, 741–771 (2017).
[28]M. Bassenne, M. Esmaily, D. Livescu, P. Moin, and J. Urzay, "A dynamic spectrally enriched subgrid-scale model for preferential concentration in particle-laden turbulence," Int. J. Multiphase Flow **116**, 270–280 (2019).
[29]P. L. Johnson, M. Bassenne, and P. Moin, "Turbophoresis of small inertial particles: Theoretical considerations and application to wall-modelled large-eddy simulations," J. Fluid Mech. **883**, A27 (2020).
[30]P. Mason and D. Thomson, "Stochastic backscatter in large-eddy simulation of boundary layers," J. Fluid Mech. **242**, 51–78 (1992).
[31]U. Piomelli *et al.*, "The inner–outer layer interface in large-eddy simulations with wall-layer models," Int. J. Heat Fluid Flow **24**, 538–550 (2003).
[32]A. Keating and U. Piomelli, "A dynamic stochastic forcing method as a wall-layer model for large-eddy simulation," J. Turbul. **7**, N12–N41 (2006).
[33]T. Schönfeld and M. Rudgyard, "Steady and unsteady flow simulations using the hybrid flow solver avbp," AIAA J. **37**, 1378–1385 (1999).

[34]N. Gourdain, L. Gicquel, M. Montagnac, O. Vermorel, M. Gazaix, G. Staffelbach, M. Garcia, J.-F. Boussuge, and T. Poinsot, "High performance parallel computing of flows in complex geometries: I. methods," Comput. Sci. Discovery **2**, 015003 (2009).
[35]L. Y. Gicquel, N. Gourdain, J. F. Boussuge, H. Deniau, G. Staffelbach, P. Wolf, and T. Poinsot, "High performance parallel computing of flows in complex geometries," C. R. Mecan. **339**, 104–124 (2011).
[36]E. Riber, V. Moureau, M. García, T. Poinsot, and O. Simonin, "Evaluation of numerical strategies for large eddy simulation of particulate two-phase recirculating flows," J. Comput. Phys. **228**, 539–564 (2009).
[37]J.-M. Senoner, M. Sanjose, T. Lederlin, F. Jaegle, M. Garcia, E. Riber, B. Cuenot, L. Gicquel, H. Pitsch, and T. Poinsot, "Eulerian and Lagrangian Large-Eddy simulations of an evaporating two-phase flow," Comptes Rendus Mécanique. **337**(6) 458–468 (2009).
[38]P. Lax and B. Wendroff, "Systems of conservation laws," Commun. Pure Appl. Math. **13**, 217–237 (1960).
[39]J. Kim, P. Moin, and R. Moser, "Turbulence statistics in fully developed channel flow at low Reynolds number," J. Fluid Mech. **177**, 133–166 (1987).
[40]J. Nikuradse, "Strömungsgesetze in rauhen rohren," Forsch. Geb. Ing. **361**, 1 (1933); available at https://citeseerx.ist.psu.edu/viewdoc/download?doi=10.1.1.467.2980&rep=rep1&type=pdf.
[41]S. Hoyas and J. Jiménez, "Reynolds number effects on the Reynolds-stress budgets in turbulent channels," Phys. Fluids **20**, 101511 (2008).
[42]G. Coleman, J. Kim, and R. D. Moser, "A numerical study of turbulent supersonic isothermal-wall channel flow," J. Fluid Mech. **305**, 159–183 (1995).
[43]R. M. So, T. B. Gatski, and T. P. Sommer, "Morkovin hypothesis and the modeling of wall-bounded compressible turbulent flows," AIAA J. **36**, 1583–1592 (1998).
[44]D. R. Chapman and G. D. Kuhn, "The limiting behaviour of turbulence near a wall," J. Fluid Mech. **170**, 265–292 (1986).
[45]S. B. Pope, *Turbulent Flows* (Cambridge University Press, 2000).
[46]L. Prandtl, "Uber die ausgebildete turbulenz," in *Proceedings of 2d International Congress of Applied Mechanics* (Zürich, 1925), pp. 62–74.
[47]T. V. Kármán, "Turbulence and Skin Friction," J. Aeronaut. Sci. **1**, 1–20 (1934).
[48]H. Schlichting and K. Gersten, *Boundary-Layer Theory* (Springer Berlin Heidelberg, 1979).
[49]G. Taylor, *Statistical Theory of Turbulence* (Royal Society, 1935).